Physics Letters B 703 (2011) 128–134

Contents lists available at ScienceDirect

Physics Letters B

www.elsevier.com/locate/physletb

Measurement of zero degree single photon energy spectra for $\sqrt{s} = 7$ TeV proton–proton collisions at LHC ☆

LHCf Collaboration

O. Adriani [a,b], L. Bonechi [a], M. Bongi [a], G. Castellini [a,b], R. D'Alessandro [a,b], A. Faus [n], K. Fukatsu [d], M. Haguenauer [f], Y. Itow [d,e], K. Kasahara [g], K. Kawade [d], D. Macina [h], T. Mase [d], K. Masuda [d], Y. Matsubara [d], H. Menjo [a,e], G. Mitsuka [d], Y. Muraki [d], M. Nakai [g], K. Noda [j], P. Papini [a], A.-L. Perrot [h], S. Ricciarini [a,c], T. Sako [d,e,*], Y. Shimizu [g], K. Suzuki [d], T. Suzuki [g], K. Taki [d], T. Tamura [i], S. Torii [g], A. Tricomi [j,k], W.C. Turner [l], J. Velasco [n], A. Viciani [a], K. Yoshida [m]

[a] *INFN Section of Florence, Italy*
[b] *University of Florence, Italy*
[c] *Centro Siciliano di Fisica Nucleare e Struttura della Materia, Catania, Italy*
[d] *Solar-Terrestrial Environment Laboratory, Nagoya University, Nagoya, Japan*
[e] *Kobayashi-Maskawa Institute for the Origin of Particles and the Universe, Nagoya University, Nagoya, Japan*
[f] *Ecole-Polytechnique, Palaiseau, France*
[g] *RISE, Waseda University, Japan*
[h] *CERN, Switzerland*
[i] *Kanagawa University, Japan*
[j] *INFN Section of Catania, Italy*
[k] *University of Catania, Italy*
[l] *LBNL, Berkeley, CA, USA*
[m] *Shibaura Institute of Technology, Japan*
[n] *IFIC, Centro Mixto CSIC-UVEG, Spain*

ARTICLE INFO

Article history:
Received 28 April 2011
Received in revised form 12 July 2011
Accepted 26 July 2011
Available online 3 August 2011
Editor: M. Doser

Keywords:
LHC
Ultra-high energy cosmic-ray
Hadron interaction models

ABSTRACT

In early 2010, the Large Hadron Collider forward (LHCf) experiment measured very forward neutral particle spectra in LHC proton–proton collisions. From a limited data set taken under the best beam conditions (low beam-gas background and low occurrence of pile-up events), the single photon spectra at $\sqrt{s} = 7$ TeV and pseudo-rapidity (η) ranges from 8.81 to 8.99 and from 10.94 to infinity were obtained for the first time and are reported in this Letter. The spectra from two independent LHCf detectors are consistent with one another and serve as a cross check of the data. The photon spectra are also compared with the predictions of several hadron interaction models that are used extensively for modeling ultra-high energy cosmic-ray showers. Despite conservative estimates for the systematic errors, none of the models agree perfectly with the measurements. A notable difference is found between the data and the DPMJET 3.04 and PYTHIA 8.145 hadron interaction models above 2 TeV where the models predict higher photon yield than the data. The QGSJET II-03 model predicts overall lower photon yield than the data, especially above 2 TeV in the rapidity range $8.81 < \eta < 8.99$.

1. Introduction

The lack of knowledge about forward particle production in hadron collisions affects the interpretation of observations of Ultra-High Energy Cosmic-Rays (UHECR). Although UHECR observations have made notable improvements in the last few years [1–7], some critical parts of the analysis depend on the Monte Carlo (MC) simulations of air shower development that are sensitive to the choice of the hadron interaction model. Accelerator data on the production of very forward emitted particles are indispensable for constraining the hadron interaction models but are usually not available from the large general purpose detectors. The Large Hadron Collider forward (LHCf) experiment has been designed to

☆ © CERN, for the benefit of the LHCf Collaboration.

* Corresponding author at: Solar-Terrestrial Environment Laboratory, Nagoya University, Nagoya, Japan.
E-mail address: sako@stelab.nagoya-u.ac.jp (T. Sako).

0370-2693/
doi:10.1016/j.physletb.2011.07.077

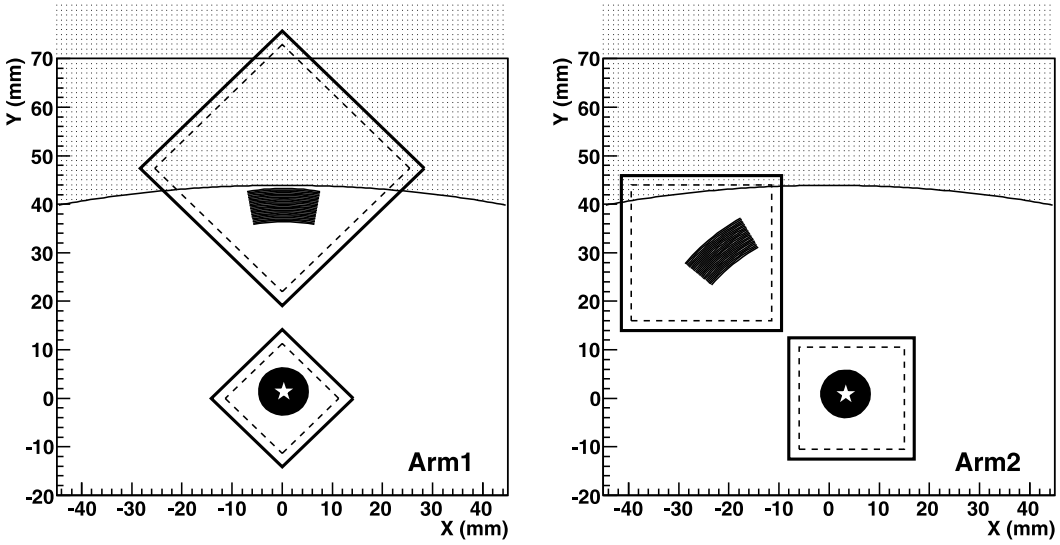

Fig. 1. Cross sections of the calorimeters seen from IP1, left for Arm1 and right for Arm2. The origin of the coordinates is defined as the zero degree collision angle in the ideal case while the stars indicate the actual zero degree found in the experimental data. The shaded area over Y = 40 mm is behind the projection of the beam pipe in case of 0 beam crossing angle where the calorimeters are insensitive to the collision products. Dashed lines in the calorimeters indicate the boarder of the 2 mm edge cut as described in Section 3.1 and the dark areas indicate common rapidity ranges of the two Arms selected to obtain the final spectra.

measure the neutral particle production cross sections at very forward collision angles of LHC proton–proton collisions, including zero degrees. When the LHC reaches its designed goal of 14 TeV collision energy, the energy in the equivalent laboratory frame will be 10^{17} eV, a factor of one thousand increase compared to previous accelerator data in the very forward regions [8,9].

Two detectors, called Arm1 and Arm2, have been installed in the instrumentation slots of the TANs (Target Neutral Absorbers) located ±140 m from the ATLAS interaction point (IP1) and at zero degree collision angle. Inside a TAN the beam vacuum chamber makes a Y shaped transition from a single common beam tube facing the IP to two separate beam tubes joining to the arcs of LHC. Charged particles from the IP are swept aside by the inner beam separation dipole D1 before reaching the TAN so only neutral particles are incident on the LHCf detectors. This unique location covers the pseudo-rapidity range from 8.7 (8.4 in case of the operation with the maximum beam crossing angle) to infinity (zero degrees). Each detector has two sampling and imaging calorimeters composed of 44 radiation lengths (1.55 hadron interaction lengths) of tungsten and 16 sampling layers of 3 mm thick plastic scintillators. The transverse sizes of the calorimeters are 20 mm × 20 mm and 40 mm × 40 mm in Arm1, and 25 mm × 25 mm and 32 mm × 32 mm in Arm2. The smaller calorimeters cover the zero degree collision angle. The cross sections of the calorimeters seen from IP1 are illustrated in Fig. 1. Four X–Y layers of position sensitive detectors (scintillating fiber, SciFi, belts in Arm1 and silicon micro-strip sensors in Arm2; 1 mm and 0.16 mm readout pitches, respectively) are inserted in order to provide transverse positions of the showers. The LHCf detectors have energy and position resolutions for the electromagnetic showers better than 5% and 200 μm, respectively, in the energy range >100 GeV. More detail on the scientific goals, construction and performance of the detectors can be found in previous reports [10–15].

This Letter describes the first analysis results of LHCf data. Single photon energy spectra are reported for $\sqrt{s} = 7$ TeV proton–proton collisions. In Section 2 the data set used in the analysis is introduced. In Section 3 the analysis process and experimental results are presented. Beam related background and uncertainties are discussed in Section 4. The experimental results are compared with MC predictions of several hadron interaction models in Section 5 and summarized in Section 6.

2. Data

Data used in this analysis was obtained on 15 May 2010 during proton–proton collisions at $\sqrt{s} = 7$ TeV with zero degree beam crossing angle (LHC Fill 1104). The total luminosity of the three crossing bunches in this fill, $L = (6.3\text{–}6.5) \times 10^{28}$ cm^{-2} s^{-1}, provided ideal operating conditions as discussed in Section 4. The data that were taken during a luminosity optimization scan were eliminated from the analysis. The trigger for LHCf events was generated at three levels. The first level trigger (L1T) was generated from beam pickup signals (BPTX) when a bunch passed IP1. A shower trigger was generated when signals from any successive 3 scintillation layers in any calorimeter exceeded a predefined threshold. Then the second level trigger for shower events (L2TA) was issued when the data acquisition system was armed. The threshold was chosen to achieve >99% efficiency for >100 GeV photons. Data were recorded with the third level trigger (L3T) when all the other types of second level triggers (pedestal, laser calibration, etc.) were combined. Examples of the longitudinal and lateral development of electromagnetic showers observed in the Arm2 detector are shown in Fig. 2. In this case two electromagnetic showers from π^0 decay into two photons are shown, with each photon striking a different calorimeter of the Arm2 detector. The generation of the L2TA and L3T triggers, and hence the data recording, were performed independently for the Arm1 and Arm2 detectors. Data acquisition was carried out under 85.7% (Arm1) and 67.0% (Arm2) average livetimes (ϵ_{DAQ}). The livetimes were defined as $\epsilon_{DAQ} = N_{L2TA}/N_{shower}$ where N_{shower} and N_{L2TA} are the number of counts in the shower and L2TA triggers, respectively.

The integrated luminosities ($\int L\,dt$) corresponding to the data used in this Letter are 0.68 nb^{-1} (Arm1) and 0.53 nb^{-1} (Arm2) after the data taking livetimes are taken into account. The absolute luminosity is derived from the counting rate of the Front Counters (FC) [11]. FCs are thin plastic scintillators fixed in front of the LHCf main calorimeters and covering a wide aperture of 80 mm × 80 mm. The calibration of the FC counting rates to the absolute luminosity was made during the Van der Meer scans on

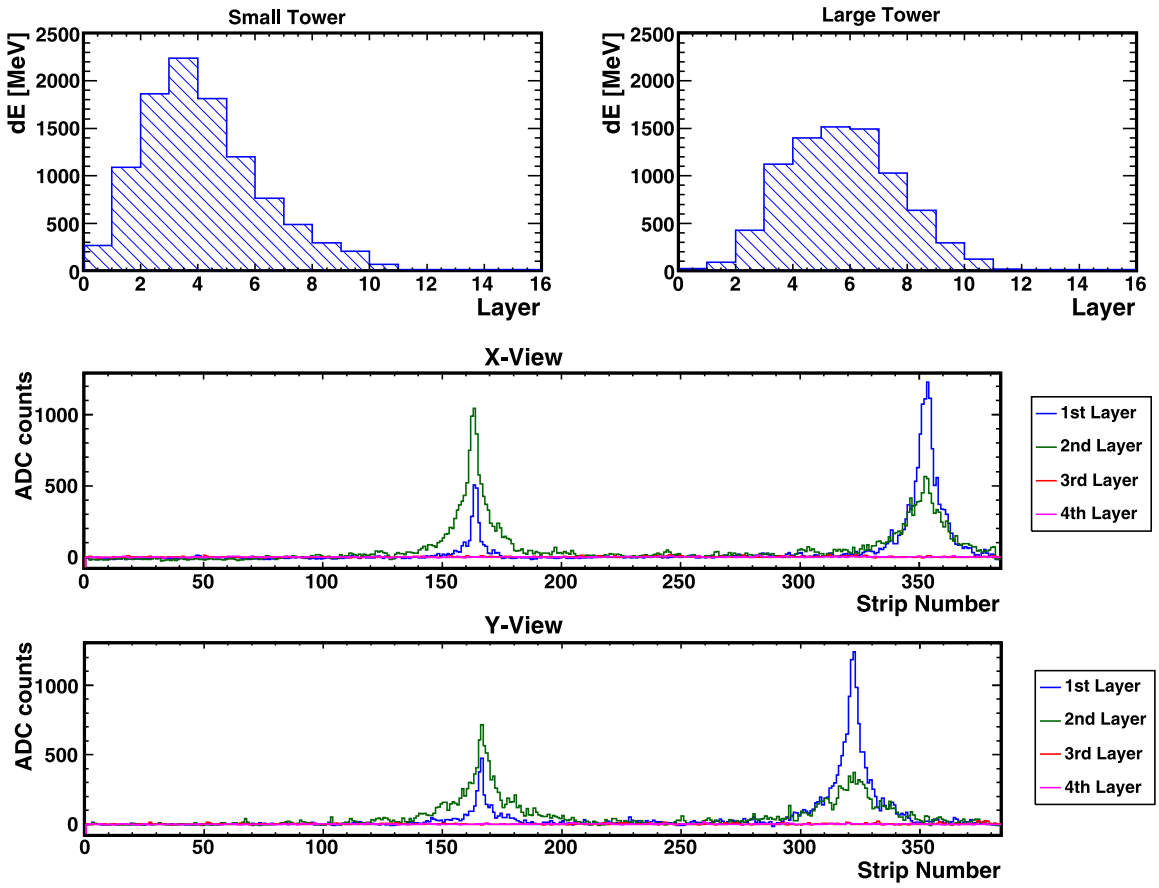

Fig. 2. An example of the π^0 candidate events observed in the LHCf Arm2 detector. Top two figures show the longitudinal developments of the two photon initiated showers observed in the 25 mm and the 32 mm calorimeters. In the middle and bottom panels, transverse X and Y profiles of the showers are shown. Different colors indicate data in the different silicon layers. (For interpretation of the references to color in this figure legend, the reader is referred to the web version of this Letter.)

26 April and 9 May 2010. The calibration factors obtained from the two scans differ by 2.1%. The estimated luminosities for the 15 May data differ by 2.7% between the two FCs. Considering the uncertainty of ±5.0% in the beam intensity measurement during the Van der Meer scans [16], we estimate an uncertainty of ±6.1% in the luminosity determination.

3. Analysis and results

3.1. Event reconstruction

The same analysis process has been adapted to each Arm independently. The transverse impact position of a particle is determined using the information provided by the position sensitive detectors. Using the position information, the raw data from the scintillation layers are corrected for the non-uniformity of light collection and for shower 'leakage out' the edges of the layers [12]. Events that fall within 2 mm of the edges are removed from the analysis due to the large uncertainty in the energy determination owing to shower leakage. The recorded charge information is converted to deposited energy based on calibration runs with SPS fixed target experiments below 200 GeV [10,13]. The sum of the energy deposited in the 2nd–13th scintillation layers is converted to the primary photon energy by using a function determined by MC simulation using the EPICS 8.81/COSMOS 7.49 simulation package [17] and confirmed in the SPS beam tests. Note that this energy estimate does not represent the incident energy of hadrons because our calorimeters have only 1.55 hadron interaction lengths. In the detector simulations the Landau–Pomeranchuk–Migdal effect [18,19] has been considered and neglecting the LPM effect does not change the energy estimate at the 1% level because we sum the deposited energy up to a sufficiently deep layer.

The linearity of each PMT was carefully tested before detector assembly over a wide range of signal amplitude by exciting a scintillator using a 337 nm UV laser pulse [10,12]. Although the measured non-linear response functions have been applied in the analysis, the difference between linear and non-linear reconstructions for 3 TeV photons is only 0.5% at maximum. We also took data under LHC conditions with different PMT gains, but after applying gain calibrations no difference in the data sets was observed. Events having energy below 100 GeV are eliminated from the analysis to avoid corrections due to the trigger inefficiency and to reject particles produced in the interaction between collision products and the beam pipe.

3.2. Single event selection

Almost all photons observed by the LHCf calorimeters are produced from the decay of π^0 and η mesons generated in the collisions. The target of our analysis is to obtain the energy spectra of these photons. To deduce the single photon energy, multi-hit events with more than one photons registered in a single calorimeter are eliminated. These multi-hit events are identified by using the lateral shower distribution measured by the position sensitive layers. According to MC simulation, the efficiency for correctly identifying true single photon events is >98%. The efficiency for identifying multi-hit events depends on the distance and the

energy ratio of two photons and the detectors because of the different readout pitches of the Arm1 SciFi belts and the Arm2 silicon micro-strip sensors. When the separation is greater than 1 mm and the lower energy photon has more than 5% of the energy of the nearby photon, the efficiencies for identifying multi-hit events are >70% and >90% for Arm1 and Arm2, respectively.

To estimate the systematic uncertainty in the multi-hit identification efficiency, we produced an artificial sample of multi-hit event sets by superimposing two clearly single photon-like events for both the experimental and MC data based on the EPOS 1.99 model [20]. Details of the MC simulations are described in Section 5. To choose the energies and separation of a photon pair, we followed the distributions determined by the DPMJET 3.04 model [21]. For the two artificial data sets the efficiencies for identifying multi-hit events do not differ by more than 10% and 3% over the entire energy range for Arm1 and Arm2, respectively. This affects the final single photon energy spectrum shape by less than 1% below 1.5 TeV and increasingly up to 2–20% at 3 TeV. The maximum difference is found for the Arm1 large calorimeter.

Next, we compared the effect of the multi-hit cut on the Arm1 and Arm2 detectors. While the fraction of events thrown out by this cut differs by less than 5% between 0.5 TeV and 1.5 TeV, it gradually increases to 30% and 60% at 3 TeV for the small and large calorimeters, respectively. The main reason for these differences is the different geometry of the Arm1 and Arm2 calorimeters. The different performances of the position sensitive detectors in the two Arms and an uncertainty in the absolute energy scale discussed in Section 3.4 may also contribute to the differences in multi-hit identification fractions of the Arm1 and Arm2 detectors. Because we cannot presently separate the sources of the difference and hence cannot apply corrections to the data, we assign the differences divided by $\sqrt{2}$ as part of the systematic uncertainty for each detector. Finally we take quadratic sum of the two uncertainties related to the multi-hit identification efficiency and the multi-hit cut as systematic error of the single photon selection procedure.

3.3. Photon event selection

To select only electromagnetic showers and eliminate hadron (predominantly neutron) contamination, a simple parameter, $L_{90\%}$ is defined. $L_{90\%}$ is the longitudinal distance in radiation lengths measured from the entrance to a calorimeter to the position where 90% of the total shower energy has been deposited. Fig. 3 shows the distribution of $L_{90\%}$ for the 20 mm calorimeter of the Arm1 detector for the events with the reconstructed energy between 500 GeV and 1 TeV. Two distinct peaks are observed corresponding to photon and hadron (neutron) events. The $L_{90\%}$ distributions for pure photon and hadron samples are generated by MC simulation using the collision product generator QGSJET II-03 [22] as shown in Fig. 3. They are called 'templates' hereafter. The choice of hadron interaction model in determining the template does not affect the results in this Letter. In the event selection, we set an energy dependent criteria in $L_{90\%}$ to keep the photon detection efficiency $\epsilon_{PID} = 90\%$ over the entire energy range based on the photon template. The purity of the selected photon events is determined by normalizing the template functions to the observed $L_{90\%}$ distribution. The purity, P, is defined as $P = N_{phot}/(N_{phot} + N_{had})$ in each energy bin. Here N_{phot} and N_{had} are the numbers of photon and hadron (neutron) events in the templates in the selected $L_{90\%}$ range. Multiplying each energy bin by $P \times \epsilon_{PID}^{-1}$, we obtained non-biased photon energy spectra.

Some disagreements in the $L_{90\%}$ distribution are found between the data and the MC calculations. This may be caused by errors in the absolute energy determination and channel-to-channel calibrations and may also be motivation for studying the LPM effect in detail. Here we consider a systematic uncertainty caused by the uncertainty of the template fitting method in the correction of the photon spectra. Small modifications of the template functions, widening with respect to the peak position up to 20% and constant shift up to 0.7 radiation lengths, to give the best match with the data, provide another estimate of the correction to the photon spectra. The difference of the correction factors between the original and the modified template methods amount to 5–20% from low to high photon energy and this is assigned as a systematic uncertainty of the particle identification in the final spectra.

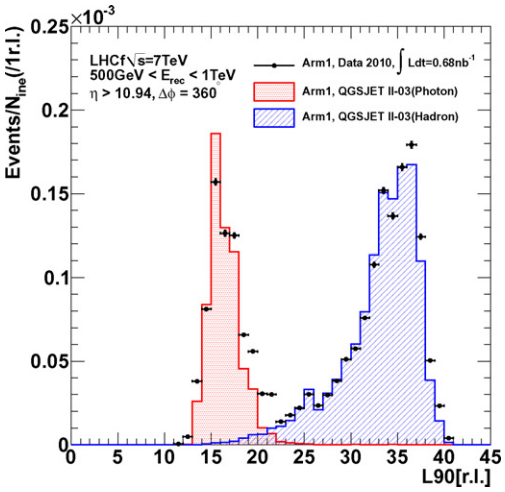

Fig. 3. The $L_{90\%}$ distribution measured by the Arm1 20 mm calorimeter for the reconstructed energy of 500 GeV–1 TeV. Plots are experimental data and the red and blue histograms are the templates calculated from the pure photon and pure hadron MC events, respectively. The two templates are independently normalized to best describe the observed data. (For interpretation of the references to color in this figure legend, the reader is referred to the web version of this Letter.)

3.4. Energy scale uncertainty from π^0 mass reconstruction

When each of two calorimeters records a single photon as shown in Fig. 2, shower 'leakage in' is corrected according to a function based on MC simulation. Using the corrected energies and positions of the shower axes, the invariant mass of the photon pair is calculated assuming their vertex is at the interaction point. In MC simulations of the full detector response and the analysis process, we confirmed the reconstructed mass peaks at 135.2 MeV in Arm1 and 135.0 MeV in Arm2, thus reproducing the π^0 mass. The statistical uncertainty in the reconstructed invariant mass of the MC simulations is ±0.2 MeV.

On the other hand, the reconstructed invariant masses of photon pairs for the experimental data are 145.8 ± 0.1 MeV (Arm1) and 140.0 ± 0.1 MeV (Arm2) where ±0.1 MeV uncertainties are statistical. A portion of the 7.8% and 3.7% invariant mass excess compared to the π^0 mass reconstructed in the MC simulations can be explained by the well understood systematic error of the absolute energy scale, estimated to be ±3.5%. This 3.5% systematic error is dominated by the errors in factors converting measured charge to deposited energy and by the errors in corrections for non-uniform light collection efficiency. Uncertainties in determining the opening angle of a photon pair and the shower leakage-in correction, typically ±1% and ±2% respectively, are also sources of error in mass reconstruction. These known elements quadratically add up to a systematic mass shift of 4.2% and can explain the mass shift in the Arm2 detector, but not Arm1.

Because all the two photon invariant mass shift may not be due to the energy scale uncertainty, we did not apply any correction for

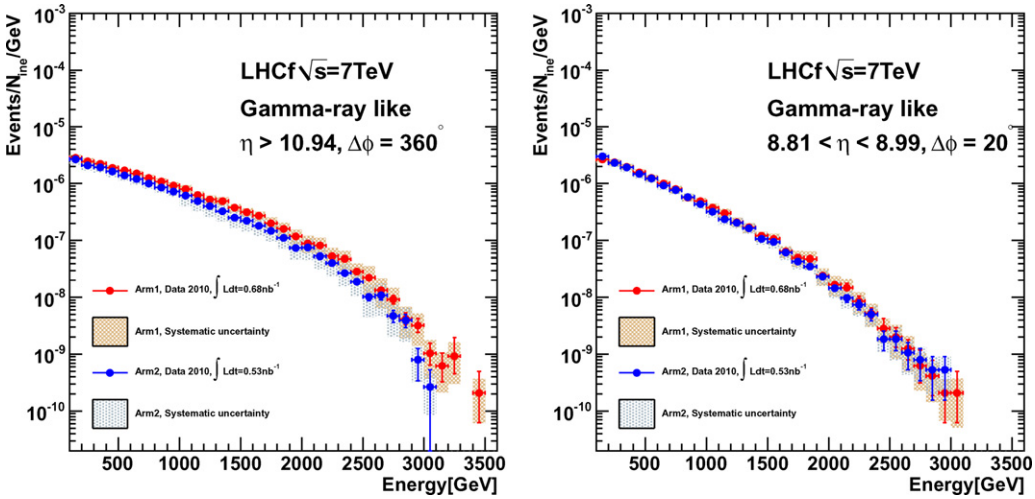

Fig. 4. Single photon spectra measured by the Arm1 (red) and Arm2 (blue) detectors. Left (right) panel shows the results for the small (large) calorimeter or large (small) rapidity range. The error bars and shaded areas indicate the statistical and systematic errors, respectively. To discuss consistency of two detectors, only uncorrelated components are plotted for the systematic errors. (For interpretation of the references to color in this figure legend, the reader is referred to the web version of this Letter.)

energy scale in the energy spectra presented in Section 3.5. Instead we assigned asymmetric systematic errors in the absolute energy scale, [−9.8%, +1.8%] (Arm1) and [−6.6%, +2.2%] (Arm2). Here we assumed uniform and Gaussian probability distributions for the energy scale errors estimated from the mass shift (7.8% and 3.7%) and the known systematics (3.5%), respectively. After the standard deviations of two components ($7.8\%/\sqrt{3}$ in case of the uniform probability distribution) were quadratically added, the systematic error bands are assigned with respect to the central value of the mass shift. To determine the systematic errors in the final energy spectra, we reconstructed two energy spectra by scaling the energy using the two extremes quoted above. The differences from the non-scaled spectrum to the two extreme spectra are assigned as systematic errors in each energy bin.

3.5. Spectra reconstruction

To compensate for the different geometry of the two arms, we selected common rapidity and azimuthal ranges to deduce the photon energy spectra. The ranges used for the small calorimeters and the large calorimeters are [$\eta > 10.94$, $\Delta\phi = 360.0°$] and [$8.99 > \eta > 8.81$, $\Delta\phi = 20.0°$], respectively. Here η and $\Delta\phi$ represent the pseudo-rapidity and interval in the azimuthal direction with respect to the beam axis which is centered on the small calorimeters. These selected areas are indicated as dark areas in Fig. 1.

Photon spectra measured in the small and large calorimeters are shown in Fig. 4. The red and blue plots show the results from Arm1 and Arm2, respectively. The error bars and shaded areas indicate the one standard deviation statistical and systematic errors, respectively, uncorrelated between the two detectors. On the vertical axis, the number of inelastic collisions, N_{ine}, is calculated as $N_{ine} = \sigma_{ine} \int L\,dt$ assuming the inelastic cross section $\sigma_{ine} = 71.5$ mb. According to the recent measurement by ATLAS [23], $\sigma_{ine} = (69.4 \pm 2.4 \pm 6.9)$ mb (first error for experimental and the second error for the extrapolation uncertainty from the limited to full phase space) was reported. They also summarized that the theoretical predictions range from 60 to 77 mb. These numbers validate our assumption of 71.5 mb and the ±10% uncertainty does not affect our final conclusions. Using the integrated luminosities introduced in Section 2, $N_{ine} = 4.9 \times 10^7$ for Arm1 and 3.8×10^7 for Arm2. From Fig. 4 we find general agreement between the two Arms that are within the errors. The reason for the difference between the two Arms in the small calorimeters (higher rapidity) is not yet understood. However, because the difference is still within the errors, we did not apply any correction.

Here we note that the obtained spectra are expected to be distorted from the single photon inclusive spectra due to the analysis processes especially the multi-hit cut that reflects the physical size of the LHCf detector and the differences between the hadron interaction models. The multi-hit cut is expected to suppress the event rate per pp interaction while the inefficiency of multi-hit identification raises the event rate at high energy because we misreconstruct multi photon energy as single photon energy. To estimate the deformation of the energy spectra the reconstructed energy spectra of photons normalized to the true inclusive single photon spectra are studied by MC simulations for the different hadron interaction models. Here in calculating the 'true inclusive single photon spectra,' particle decay in the 140 m flight path from the interaction point to the LHCf detectors and the LHCf calorimeter aperture are taken into account. In the case of multi-hits in a single calorimeter, each photon is counted independently. As a result, 0–15% of energy independent suppression is found below 2 TeV and it turns to gradually rise up to +15% over 3 TeV. The maximum difference between interaction models and between the two arms are about 10% and 5%, respectively.

4. Beam related background and uncertainties

The events containing more than one collision (pile-up events) in a single bunch crossing may cause an additional bias. Given that a collision has occurred, the probability of pile-up ($P(n \geqslant 2)/P(n \geqslant 1)$) can be calculated from the Poisson probability distribution. Using the highest bunch luminosity of $L = 2.3 \times 10^{28}$ cm^{-2} s^{-1} used in this analysis, inelastic cross section $\sigma_{ine} = 71.5$ mb and the revolution frequency of LHC $f_{rev} = 11.2$ kHz, the probability is $P(n \geqslant 2)/P(n \geqslant 1) = 0.072$. Considering the acceptance of a LHCf calorimeter for an inelastic collision, ∼0.03, only 0.2% of events have more than one event due to the pile-up and they are eliminated in the multi-hit cut. We conclude that pile-up does not affect our analysis.

In the geometrical analysis of the data, we assumed the projected position of the zero degree collision angle at the LHCf detectors, referred to as the 'beam-center' hereafter, can move from fill to fill owing to slightly different beam transverse position and crossing angles at the IP. We determined the 'beam center' at the

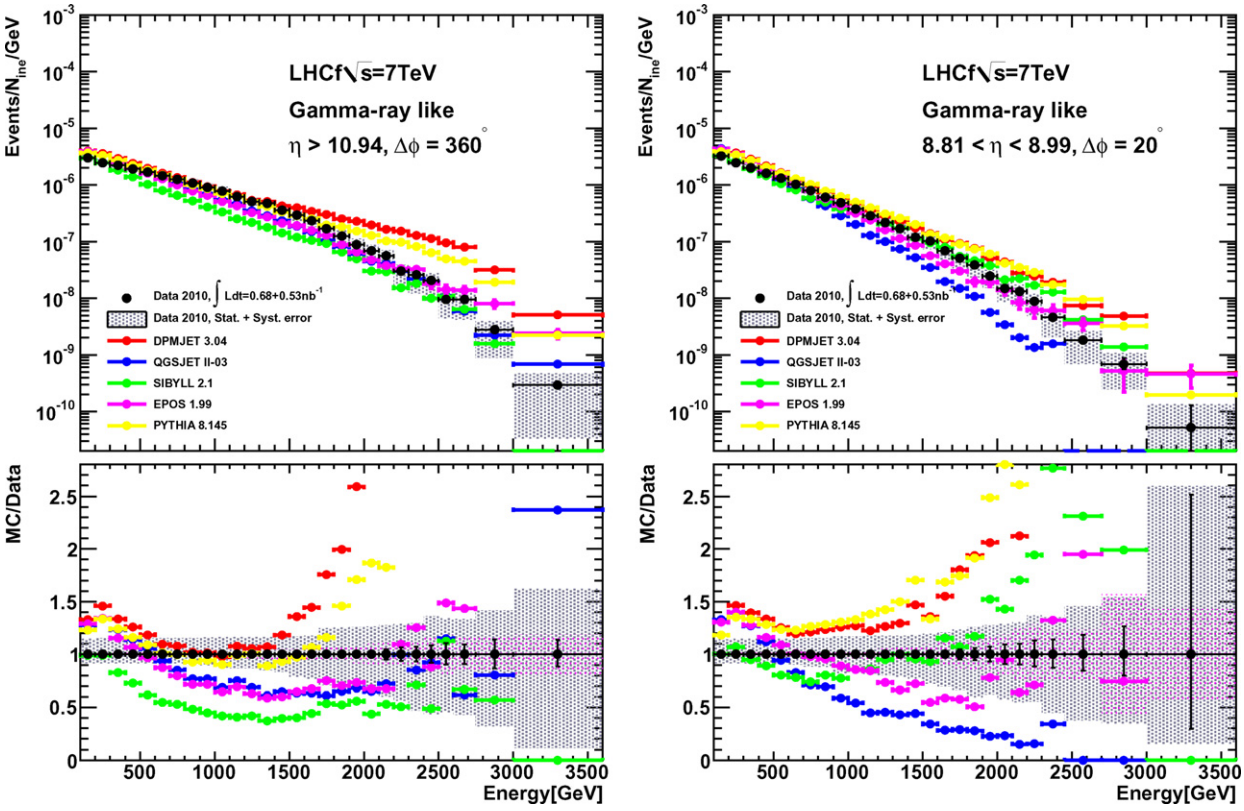

Fig. 5. Comparison of the single photon energy spectra between the experimental data and the MC predictions. Top panels show the spectra and the bottom panels show the ratios of MC results to experimental data. Left (right) panel shows the results for the large (small) rapidity range. Different colors show the results from experimental data (black), QGSJET II-03 (blue), DPMJET 3.04 (red), SIBYLL 2.1 (green), EPOS 1.99 (magenta) and PYTHIA 8.145 (yellow). Error bars and gray shaded areas in each plot indicate the experimental statistical and the systematic errors, respectively. The magenta shaded area indicates the statistical error of the MC data set using EPOS 1.99 as a representative of the other models. (For interpretation of the references to color in this figure legend, the reader is referred to the web version of this Letter.)

LHCf detectors by two methods; first by using the distribution of particle impact positions measured by the LHCf detectors and second by using the information from the Beam Position Monitors (BPMSW) installed ±21 m from the IP [24]. From the analysis of the fills 1089–1134, we found a maximum ∼4 mm shift of the beam center at the LHCf detectors, corresponding to a crossing angle of ∼30 μrad assuming the beam transverse position did not change. The two analyses gave consistent results for the location of the beam center on the detectors within 1 mm accuracy. In the geometrical construction of events we used the beam-center determined by LHCf data. We derived photon energy spectra by shifting the beam-center by 1 mm. The spectra are modified by 5–20% depending on the energy and the rapidity range. This is assigned as a part of systematic uncertainty in the final energy spectra.

The background from collisions between the beam and the residual gas in the vacuum beam pipe can be estimated from the data. During LHC operation, there were always bunches that did not have a colliding bunch in the opposite beam at IP1. We call these bunches 'non-crossing bunches' while the normal bunches are called as 'crossing bunches.' The events associated with the non-crossing bunches are purely from the beam-gas background while the events with the crossing bunches are mixture of beam-beam collisions and beam-gas background. Because the event rate of the beam-gas background is proportional to the bunch intensity, we can calculate the background spectrum contained in the crossing bunch data by scaling the non-crossing bunch events. We found the contamination from the beam-gas background in the final energy spectrum is only ∼0.1%. In addition the shape of the energy spectrum of beam-gas events is similar to that of beam-beam events, so beam-gas events do not have any significant impact on the beam-beam event spectrum.

The collision products and beam halo particles can hit the beam pipe and produce particles that enter the LHCf detectors. However according to MC simulations, these particles have energy below 100 GeV [10] and do not affect the analysis presented in this Letter.

5. Comparison with models

In the top panels of Fig. 5 photon spectra predicted by MC simulations using different models, QGSJET II-03 (blue) [22], DPMJET 3.04 (red) [21], SIBYLL 2.1 (green) [25], EPOS 1.99 (magenta) [20] and PYTHIA 8.145 (default parameter set; yellow) [26,27] for collisions products are presented together with the combined experimental results. To combine the experimental data of the Arm1 and Arm2 detectors, the content in each energy bin was averaged with weights by the inverse of errors. The systematic uncertainties due to the multi-hit cut, particle identification (PID), absolute energy scale and beam center uncertainty are quadratically added in each energy bin and shown as gray shaded areas in Fig. 5. The uncertainty in the luminosity determination (±6.1% as discussed in Section 2), that is not shown in Fig. 5, can make an energy independent shift of all spectra.

In the MC simulations, 1.0×10^7 inelastic collisions were generated and the secondary particles transported in the beam pipe. Deflection of charged particles by the D1 beam separation dipole, particle decay and particle interaction with the beam pipe are

taken into account. The responses of the detectors were calculated using the EPICS/COSMOS libraries taking the random fluctuation equivalent to electrical noise into account. The same analysis procedures were then applied to the MC simulations as to the experimental data except for the particle identification and its correction. In the analysis of the MC data set, we used the known information of the particle type. In the bottom panels the ratios of MC simulations to the experimental data are plotted together with the statistical and systematic uncertainties of the experimental data. The statistical uncertainty of the EPOS 1.99 model is also plotted as magenta shaded areas as a representative of the various models.

We find that none of the models lies within the errors of our data over the entire energy range. Some remarkable features are:

1) DPMJET 3.04 and PYTHIA 8.145 show very good agreement with the experimental result between 0.5 and 1.5 TeV for $\eta > 10.94$, but they predict significantly larger photon yield at high energy >2 TeV in both rapidity ranges.
2) QGSJET II-03 predicts overall lower photon yield than the experimental result. This is significant above 2 TeV in the rapidity range $8.81 < \eta < 8.99$.
3) For $\eta >$10.94, SIBYLL 2.1 shows a very good agreement with the experimental result for the spectral shape for >0.5 TeV, but predicts a photon yield only half of the experimental result over the entire energy range.

6. Summary

LHCf has measured for the first time the single photon energy spectra of high energy photons in the very forward region of proton–proton collisions at LHC. After selecting data with common rapidity ranges, the two independent LHCf detectors (Arm1 and Arm2) installed on either side of IP1 gave consistent results in two rapidity ranges even though the geometrical acceptances of the two detectors differ. The combined spectra of the two detectors are compared with the prediction of various hadron interaction models. It is found that none of the model predictions have perfect agreement with the experimental results within statistical and systematic errors.

The conservative systematic errors assigned in this analysis will be improved upon in future studies. In addition studies of other measurements like the inclusive single photon spectra, inclusive single π^0 and neutron production spectra, and neutral particle transverse momentum spectra are now ongoing using the already accumulated LHCf data. By combining the LHCf data with the recent studies on particle production in the central rapidity region of LHC collisions [28] it is now for the first time possible to make critical tests of hadron interaction models by using collider data over a very wide rapidity range.

Acknowledgements

We thank the CERN staff and the ATLAS Collaboration for their essential contributions to the successful operation of LHCf. Especially we appreciate continuous review of the experiment by Michelangelo Mangano, Carsten Niebuhr and Mario Calvetti. We also thank Tanguy Pierog for a quick verification of our MC calculations. This work is partly supported by Grant-in-Aid for Scientific Research by MEXT of Japan, the Mitsubishi Foundation in Japan and INFN in Italy. The receipts of JSPS Research Fellowship (H.M. and T.M.), INFN fellowship for non-Italian citizens (H.M. and K.N.) and the GCOE Program of Nagoya University "QFPU" from JSPS and MEXT of Japan (G.M.) are also acknowledged. A part of this work was performed using the computer resource provided by the Institute for the Cosmic-Ray Research (ICRR), University of Tokyo.

References

[1] J. Abraham, et al., Phys. Rev. Lett. 101 (2008) 061101.
[2] P. Abreu, et al., Astropart. Phys. 34 (2010) 314.
[3] J. Abraham, et al., Phys. Rev. Lett. 104 (2010) 091101.
[4] R. Abbasi, et al., Astropart. Phys. 32 (2009) 53.
[5] R. Abbasi, et al., arXiv:1002.1444v1, 2010.
[6] R. Abbasi, et al., arXiv:0910.4184 [astro-ph], 2009.
[7] H. Sagawa, et al., in: Proceedings of the Symposium on the Recent Progress of Ultra-High Energy Cosmic-Ray Observation 2010, Nagoya, in: AIP Conf. Proc., vol. 1367, in press.
[8] W. Flauger, F. Mönnig, Nucl. Phys. B 109 (1976) 347.
[9] E. Paré, et al., Phys. Lett. B 242 (1990) 531.
[10] LHCf Technical Design Report, CERN-LHCC-2006-004.
[11] O. Adriani, et al., JINST 3 (2008) S08006.
[12] T. Sako, et al., NIM A 578 (2007) 146.
[13] T. Mase, et al., in preparation.
[14] O. Adriani, et al., JINST 5 (2010) P01012.
[15] H. Menjo, et al., Astropart. Phys. 34 (2011) 513.
[16] CERN-ATS-Note-2011-004.
[17] K. Kasahara, EPICS web page http://cosmos.n.kanagawa-u.ac.jp/.
[18] L.D. Landau, I.J. Pomeranchuk, Dokl. Akad. Nauk 92 (1965) 535.
[19] A.B. Migdal, Phys. Rev. 103 (1956) 1811.
[20] K. Werner, F.-M. Liu, T. Pierog, Phys. Rev. C 74 (2006) 044902.
[21] F.W. Bopp, J. Ranft, R. Engel, S. Roesler, Phys. Rev. C 77 (2008) 014904.
[22] S. Ostapchenko, Phys. Rev. D 74 (2006) 014026.
[23] ATLAS Collaboration, arXiv:1104.0326v1, 2011.
[24] G. Vismara, CERN-SL-2000-056 BI, 2000.
[25] E.-J. Ahn, R. Engel, T.K. Gaisser, P. Lipari, T. Stanev, Phys. Rev. D 80 (2009) 094003.
[26] T. Sjöstand, S. Mrenna, P. Skands, JHEP 0605 (2006) 026.
[27] T. Sjöstand, S. Mrenna, P. Skands, Comput. Phys. Comm. 178 (2008) 852.
[28] D. d'Enterria, et al., arXiv:1101.5596v2, 2011.